DOI: 10.1002/asia.200800218

Relationship between Carbon Nanotube Structure and Electrochemical Behavior: Heterogeneous Electron Transfer at Electrochemically Activated Carbon Nanotubes

Martin Pumera,*[a] Toshio Sasaki,[b] and Hideo Iwai[c]

Abstract: The electrochemical activation of multiwalled carbon nanotubes (MWCNTs) (at potentials of 1.5–2.0 V vs Ag/AgCl for 60–360 s) results in significantly increased rate constants (k^0_{obs}) for heterogeneous electron-transfer with $[Fe(CN)_6]^{3-/4-}$ (from 8.34×10^{-5} cm s^{-1} for as-received MWCNTs to 3.67×10^{-3} cm s^{-1} for MWCNTs that were electrochemically activated at 2.0 V for 180 s). The increase in the value of k^0_{obs} arises from the introduction of wall defects exposing edge planes of the MWCNTs, as observed by high-resolution TEM. The density of the edge plane defects increases from almost zero (for as-received MWCNTs) to 3.7% (for MWCNTs electrochemically activated at 2.0 V for 180 s). High-resolution X-ray photoelectron spectroscopy (HR-XPS), Raman spectroscopy, and electrochemical impedance spectroscopy were used to gain a better understanding of the phenomena. HR-XPS revealed that the increase in electrochemical activation potential increases the number of oxygen-containing groups on the surface of carbon nanotubes.

Keywords: carbon nanotubes · electrochemistry · electron transfer · nanostructures · photoelectron spectroscopy

Introduction

Herein we report an investigation into the reasons for increases in the observed heterogeneous electron-transfer rate constant (k^0_{obs}) of carbon nanotubes after their electrochemical activation. Since the discovery of multiwalled carbon nanotubes (MWCNTs)[1,2] and their single-walled counterparts (SWCNTs),[3,4] these nanoscale materials have attracted much attention from electrochemists because of their unique structural and electronic properties.[5–10] The important applications of carbon nanotube electrodes are the main driving force for examining the relationship between their structure and electrochemical activity.[11–14] Of particular interest is the value of k^0_{obs} for electron transfer between carbon nanotubes and well-known redox systems such as ferri/ferrocyanide.

Electrochemical activation of carbon electrodes for the enhancement of heterogeneous electron transfer has been known for a long time. The principal reasons for electrochemical activation of highly oriented pyrolytic graphite (HOPG) electrodes were studied in detail by Raman spectroscopy, scanning electron microscopy (SEM), scanning tunneling microscopy (STM), and atomic force microscopy (AFM) with the conclusion that electrochemical activation results in extensive lattice damage and exposure of edge-plane sites in HOPG.[15–17] McCreery and co-workers found a direct correlation between the 1360 cm^{-1} Raman band (D-band) and k^0_{obs} of HOPG electrodes.[15] The same group investigated the quantitative relationship between k^0_{obs} and the microstructure of graphite electrodes.[18] Electrochemical activation of carbon nanotubes was also studied previously. Wang et al.[19] demonstrated that it is possible to electrochemically activate SWCNTs and hypothesized that this

[a] Dr. M. Pumera
Biomaterial Systems Group
Biomaterials Center and International Center
for Materials Nanoarchitectonics
National Institute for Materials Science
Nanomaterials & Biomaterials Research Building
1-1 Namiki, Tsukuba, Ibaraki (Japan)
Fax: (+81) 29-860-4706
E-mail: PUMERA.Martin@nims.go.jp

[b] T. Sasaki
High Voltage Electron Microscope Laboratory
Eco-Topia Science Institute, Nagoya University
Furo-Cho, Chikusa-ku, 464-0814 Nagoya (Japan)

[c] Dr. H. Iwai
Materials Analysis Center
National Institute for Materials Science
2-1 Sengen, Tsukuba, Ibaraki (Japan)

Supporting information for this article is available on the WWW under http://dx.doi.org/10.1002/asia.200800218.

arises from the functionalization of SWCNTs with carboxylic groups. However, they found that the relationship between applied activation potential and electrode performance is not straightforward. Later, Musameh et al.[20] demonstrated that the anodic pretreatment of MWCNT-based electrodes results in an improvement of electrochemical reactivity of carbon nanotubes. It is important to note that references [19] and [20] present only electrochemical data and do not provide any spectroscopic or microscopic insight into the phenomena. Even though Musameh et al.[20] hypothesized that such enhancement of electrochemical activity of MWCNTs results from the breaking of the basal-plane end caps of arc-produced MWCNT, they did not support this claim nor show the existence of the caps in their MWCNT samples by electron microscopy.[20] Ito et al.[21] reported that it is possible to etch individual MWCNT by applying potentials higher than 1.7 V, which they clearly demonstrated by presenting optical micrographs of MWCNTs at different stages of etching. They hypothesize that etching occurs as a consequence of carbon oxidation via an intermediate that is generated when water is converted into oxygen on the surface of MWCNTs.[21] Liu et al.[22] oxidized MWCNTs electrochemically at a potential of 2 V for 30 min and 6 h and found, using transmission electron microscopy (TEM), that the ends of some MWCNTs opened after 30 min of electrooxidation, some MWCNTs were cut, and the surface of MWCNTs eroded after 6 h of electrooxidation. Unfortunately, the resolution of the TEM images in their work was not sufficient to provide any insight into the nature of such erosion. The authors proved by FTIR spectroscopy that oxygen-containing groups (carbonyl, carboxy) were introduced during electrooxidation of MWCNTs. They also found by electrochemical impedance spectroscopy that the capacitance of electrochemically oxidized MWCNTs was promoted.[22]

Abstract in Czech: Elektrochemická aktivace uhlíkových nanotrubiček (MWCNTs) (v rozmezí potenciálů 1.5–2.0 V vs Ag/AgCl po dobu 60–360 s) vede k výrazně vyšším konstantám rychlosti heterogenního přenosu elektronů (k^0_{obs}) pro $Fe(CN)_6^{3-/4-}$, z 8.34×10^{-5} cm s^{-1} pro nemodifikované MWCNTs, na 3.67×10^{-3} cm s^{-1} pro elektrochemicky aktivované MWCNTs. Elektronovou mikroskopií bylo zjištěno, že toto zvýšení k^0_{obs} je důsledkem vytvoření výrazných defektů ve stěnách MWCNTs; zastoupení těchto defektů vzrostlo z téměř nulového (pro nemodifikované MWCNT) na 3.7 % (pro elektrochemicky aktivované). Pro objasnění pozorovaných jevů byly použity metody rentgenové fotoelektronové spektroskopie s vysokám rozlišením (HR-XPS), Ramanovy spektroskopie a elektrochemické impedanční spektroskopie. HR-XPS experimenty vedly k poznání že zvýšení elektrochemického aktivačního potenciálu vede k zvýšení zastoupení uhlíkových skupin obsahující kyslík na povrchu uhlíkových nanotrubiček.

The aim of this article is to demonstrate that electrochemical activation of carbon nanotubes results in an introduction of defects into the walls of the carbon nanotubes. These defects lead to a higher density of electroactive sites and, consequently, to increased values of k^0_{obs}. We characterized electrochemically activated carbon nanotubes by cyclic voltammetry, electrochemical impedance spectroscopy, Raman spectroscopy, high-resolution transmission electron microscopy (HR-TEM), and high-resolution X-ray photoelectron spectroscopy (HR-XPS) to gain insight into the mechanism of such activation. We discuss the structural changes in carbon nanotubes and report calculations of the density of the defects on the surfaces of MWCNTs.

Results and Discussion

As-received MWCNTs were dispersed in DMF at a concentration of 1 mg mL^{-1}. Then, 5 μL of this solution was deposited on the surface of a GC electrode and allowed to dry. The MWCNT-modified electrodes were electrochemically pretreated by applying them at a fixed potential and time in phosphate buffer (50 mM, pH 7.4). The resulting electrochemically activated MWCNT electrodes were subjected to cyclic voltammetry, electrochemical impedance spectroscopy, Raman spectroscopy, HR-TEM, and HR-XPS analyses to shed light on the mechanism of such electrochemical activation.

Cyclic Voltammetry

Cyclic voltammetry was used to measure the heterogeneous electron-transfer constant k^0_{obs} of as-received and electrochemically activated MWCNTs. The value of k^0_{obs} was calculated by a method developed by Nicholson,[23] as described briefly in the Experimental Section. Electrochemically activated MWCNT electrodes show dramatically enhanced heterogeneous electron transfer, which results in a lowering of the value of ΔE_p of $[Fe(CN)_6]^{3-/4-}$. The heterogeneous electron-transfer rate constant k^0_{obs} for $[Fe(CN)_6]^{3-/4-}$ was found to be 8.34×10^{-5} cm s^{-1} for as-received MWCNTs and increased monotonically over the whole activation potential range to 3.67×10^{-3} cm s^{-1} at an activation potential of 2.00 V (measured in 0.1 M KCl; see Figure 1 A). The latter value is similar to that previously observed at electrochemically activated HOPG electrodes ($k^0_{obs}=6.5\times10^{-3}$ cm s^{-1})[15] and, therefore, one could suggest that electrochemical activation occurs as a result of the introduction of "edge-like" defects into the walls of the carbon nanotubes. The exact reason for such enhancements in k^0_{obs} is described in detail in the following sections. The influence of electrochemical activation time on k^0_{obs} at a fixed potential of 1.75 V is shown in Figure 1 B. As can be seen, k^0_{obs} increases monotonically from 1.97×10^{-3} cm s^{-1} at an activation time of 60 s to 4.04×10^{-3} cm s^{-1} at an activation time of 360 s. The electrochemical activation of MWCNTs is very reproducible; the difference in k^0_{obs} between two measurements after a period

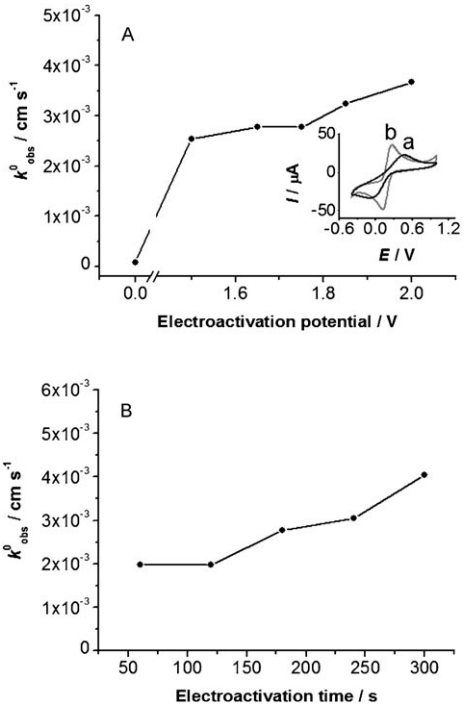

Figure 1. Effect of A) electrochemical activation potential and B) electrochemical activation time on k^0_{obs} for MWCNTs with $[Fe(CN)_6]^{3-/4-}$ in 0.1 M KCl. The inset shows cyclic voltammograms for the as-received carbon nanotubes (a, black line) and the nanotubes (b, grey line) electrochemically activated for 180 s at 1.75 V. Conditions: A) electrochemical activation time, 180 s; B) electrochemical activation potential, 1.75 V.

of three months was found to be 6.9% (k^0_{obs} of 2.59×10^{-3} and 2.77×10^{-3} cm s^{-1} for an electrochemical activation potential of 1.75 V and time of 180 s).

The relative standard deviation (RSD) of ΔE_p was in all cases less than 3% ($n=3$, measured the same day). However, for calculation of k^0_{obs}, the interpolation/extrapolation error of the Nicholson method[23] (approximately between 0 and 2%, see the Experimental Section) must be added. Since the interpolation/extrapolation error of the Nicholson method depends on ΔE_p and it is difficult to establish it exactly, we do not present RSD bars in the graphs. However, it is possible to estimate that RSD of k^0_{obs} is less than 5%.

Electrochemical Impedance Spectroscopy

It has been shown that the capacitance of highly ordered carbon materials is higher at the graphitic edges than on the basal planes.[24] It was suggested that this difference arises from the anisotropic conductivity of such materials, which under polarization build up more charge and consequently more capacitance at the plane edges as a result of the much higher electrical conductivity along the basal planes (relative to the perpendicular direction) owing to the mobility of the delocalized π electrons.[24]

Electrochemical impedance spectroscopy was used to measure the changes in capacitance of MWCNTs at different stages of electroactivation to understand the nature of the changes in MWCNT structure. The observed weight-specific capacitance of carbon nanotubes increases monotonically over the whole activation potential range (from 1.18 F g^{-1} for as-received MWCNTs to 4.75 F g^{-1} for an electroactivation potential of 2.00 V; Figure 2A). The observed weight-specific capacitance of MWCNTs also increases with increasing electroactivation time (at a fixed electroactivation potential of 1.75 V) from 2.69 F g^{-1} at an activation time of 60 s to 4.85 F g^{-1} at an activation time of 360 s (Figure 2B). The increased capacitance during electroactivation arises from a combination of the following effects: 1) The frequency of edge-like domains on the carbon nanotube surface increases. 2) Such edge-like domains increase the roughness of the carbon nanotube surface (as confirmed by HR-TEM in the following section), which increases the wetting of otherwise significantly hydrophobic MWCNT surfaces[25] and consequently decreases the distance between the solvent (water) and the surface of the nanotube. As a result of the very high dielectric constant of water, the capacitance of such "roughened" carbon nanotubes therefore increases. 3) Electrochemical activation introduces oxygen-containing groups on MWCNT surfaces (as confirmed by high-resolution XPS in the following section), which leads to increased wetting as discussed in the previous point. 4) These oxygen-containing groups are solvated by water, which again increases the capacitance of the carbon nanotubes. 5) The oxygen-containing groups at the surface of the carbon nanotubes might undergo Faradaic reactions, which would contribute to the observed capacitance. The contribution of

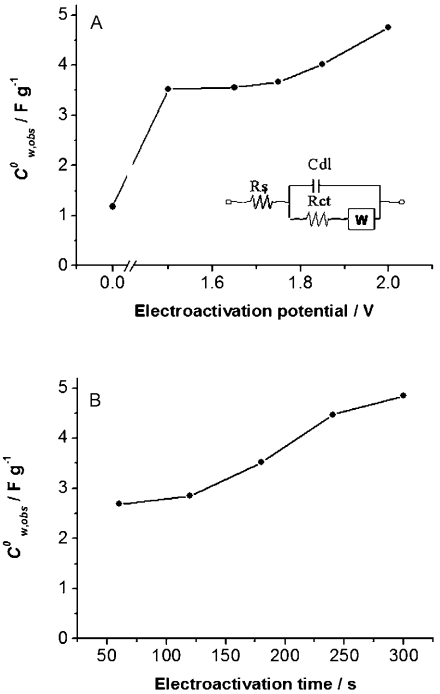

Figure 2. Effect of A) electrochemical activation potential and B) electrochemical activation time on weight-specific capacitance of carbon nanotubes. The inset shows the Randles equivalent circuit. Conditions: A) electrochemical activation time, 180 s; B) electrochemical activation potential, 1.75 V.

these effects to the capacitance is further discussed in the following sections.

The weight-specific capacitances of carbon nanotubes presented in this article are on the same order of magnitude as the weight-specific capacitances obtained by this and other authors for carbon nanotubes.[26–28]

X-ray Photoelectron Spectroscopy

XPS is a very useful tool for obtaining information on the chemical states of materials. It has proven its suitability for the chemical analysis of carbon nanotubes.[13,29–31] HR-XPS was used in this work to gain an insight into chemical state changes in as-received and electrochemically activated carbon nanotubes. HR-XPS spectra of the carbon 1s core level as well as high-resolution spectra of oxygen 1s level were recorded for as-received MWCNTs (Figure 3A) and for MWCNTs electrochemically activated for 180 s at 1.75 V (Figure S-1A, Supporting Information), at 1.85 V (Figure S-1B, Supporting Information), and at 2.00 V (Figure 3B). The XPS C 1s core spectra of MWCNTs show a single tailing peak at 284.5 eV, the maximum of which corresponds to sp^2 hybridization of graphene sheets in a carbon nanotube.[31,32] Careful curve fitting shows that the C 1s spectrum of a MWCNT can be quantitatively differentiated into five different carbon stages, namely, sp^2-hybridized carbon atoms (at 284.4 eV) of the graphene sheet of a MWCNT, sp^3-hybridized carbon atoms (-CH_2-) (at 285.2 eV), the alcohol/ether group (*C*–O) (at 286.6 eV), the carbonyl group (*C*=O) (at 288.0 eV), and the carboxy acid/ester group (O–*C*=O) (at 289.2 eV). Also present is the π–π* shake-up signal (at 290.5 eV), which is typical for sp^2-hybridized carbon (in the text and also in Figure 3, the atom that is responsible for the given signal is in italics). A quantitative comparison of the C 1s core-level spectra of an as-received and electrochemically activated MWCNT is given in Table 1 (in our calculations we exclude the π–π* shake-up signal). It is clear that

Table 1. Quantitative comparison of high-resolution X-ray photoelectron spectra of the C 1s core level at different carbon stages for as-received and electrochemically activated (for 180 s) carbon nanotubes.

Electrochemical activation potential	carbon–carbon	C–O	C=O	O–C=O
–[a]	88.7 %	6.7 %	3.6 %	1.0 %
1.75 V	87.9 %	7.4 %	3.4 %	1.4 %
1.85 V	87.8 %	8.0 %	2.6 %	1.6 %
2.00 V	61.1 %	25.3 %	7.3 %	6.3 %

[a] As received.

the relative abundance of carboxy/ester groups (O-C=O) increases from 1.0 to 6.3 % (relative increase of 630 %), alcohol/ether groups (C–O) increase from 6.7 to 25.3 % (relative increase of 377 %), and C=O increases from 3.6 to 7.3 % at the expense of the carbon–carbon groups, of which the relative abundance decreased from 88.7 to 61.1 % (relative decrease by 31 %) upon increasing the electrochemical activation potential from 0 to 2.00 V (for 180 s). Note that, in principle, the signals for carboxy acid and the ester groups cannot be distinguished by the C 1s signal because the carbon atom in these groups has the same chemical neighborhood. However, by using the HR-XPS O 1s core oxygen signal, one can distinguish between the carboxy acid/carbonyl groups (O–C=*O* and C=*O*) (at 532.2 eV) and signals from the ester groups (C–*O*–C=O) (at 533.7 eV). A quantitative comparison of the O 1s core-level spectra of an as-received and electrochemically activated MWCNT is shown in Table 2. It is clear that the relative abundance of the ester groups decreases significantly with an increase in the electrochemical activation potential while the relative presence of the signal from carboxy acid/carbonyl increases with an increase in the electrochemical activation po-

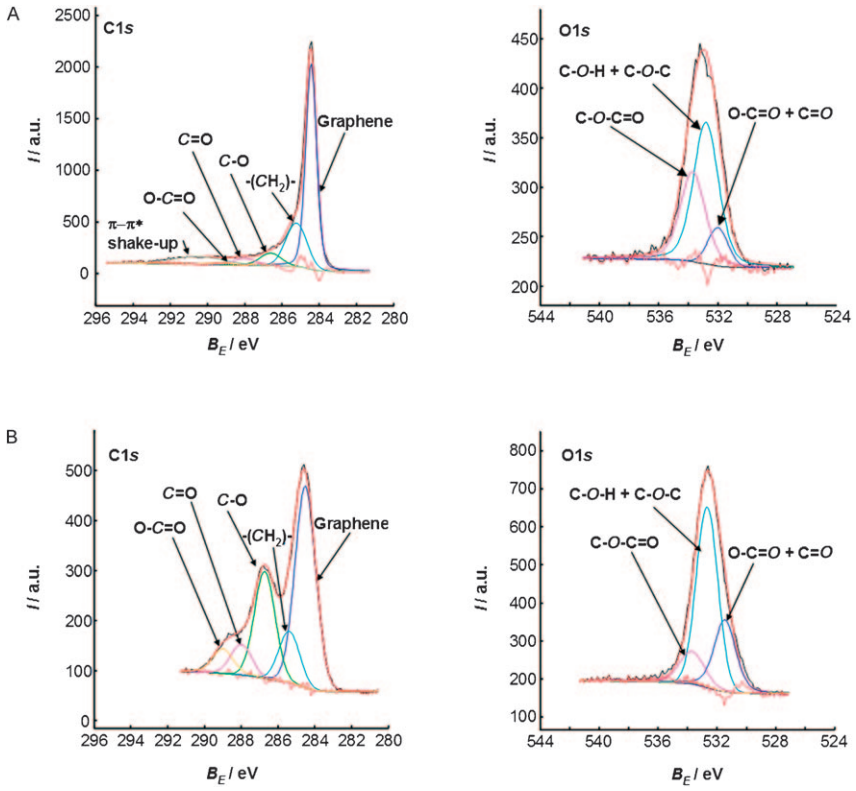

Figure 3. HR-XPS spectra of A) as-received and B) electrochemically activated carbon nanotubes at 2.00 V for 180 s. Left, C 1s core spectra; right, O 1s core spectra.

Table 2. Quantitative comparison of high-resolution X-ray photoelectron spectra of the O 1s core level at different oxygen stages for as-received and electrochemically activated (for 180 s) carbon nanotubes.

Electrochemical activation potential	O–C=O and C=O	C–O–H and C–O–C	C–O–C=O
–[a]	7.8%	55.6%	36.6%
1.75 V	10.4%	54.6%	35.0%
1.85 V	30.6%	58.2%	11.2%
2.00 V	27.1%	59.6%	13.3%

[a] As received.

tential. XPS data from the C 1s and O 1s measurements are consistent with each other and their synthesis leads us to conclude that after the electrochemical activation, there is an increase in the relative presence of carboxy groups at the expense of the relative presence of the alcohol, ether, and carbonyl groups. In this context, it is important to mention that Masheter et al.[32] recently found by XPS and voltammetry that nitric acid treatment of MWCNTs leads to a relative increase of abundance of the carboxy groups.

Here we wish to discuss the influence of oxygen-containing groups upon increasing heterogeneous electron transfer. Chou et al.[13] demonstrated that an increase in the presence of carboxy-containing groups on single-walled carbon nanotubes (induced by mineral acid treatment of SWCNTs) leads to an increase in the heterogeneous electron-transfer rate for $[Fe(CN)_6]^{3-/4-}$. Later, however, Pumera[28] demonstrated in contrast that similar treatment of single- and double-walled carbon nanotubes (DWCNTs) leads to a slower heterogeneous electron-transfer for $[Fe(CN)_6]^{3-/4-}$, more strongly in the case of SWCNTs and less intensely in the case of DWCNTs. Ji et al.[33] studied the influence of oxygen-containing groups of graphite electrodes in great detail and found that heterogeneous electron transfer for $[Fe(CN)_6]^{3-/4-}$ at graphite is actually slowed by increasing the amount of oxygen-containing groups at graphite electrodes. Later, the same group demonstrated that even for MWCNTs, the increase of oxygenated species may not increase electron-transfer kinetics.[34] In our present case, the highest relative increase of oxygen-containing groups upon electrochemical activation of pristine MWCNTs at 2.00 V for 180 s is 630% (for carboxy groups). There is a clear correlation between the abundance of oxygen-containing groups and the heterogeneous electron-transfer rate constant (see Figure S-2, Supporting Information), although this correlation is not linear, suggesting that oxygen-containing groups are not solely responsible for the increasing value of k^0_{obs}. In addition, the value of k^0_{obs} for $[Fe(CN)_6]^{3-/4-}$ was found to increase by two orders of magnitude (from 8.34×10^{-5} to 3.67×10^{-3} cm s^{-1}). If oxygen-containing groups were solely responsible for the increase of k^0_{obs}, the increase would be much smaller (about ten times). Therefore, we conclude that oxygen-containing groups play a minor role in enhancing heterogeneous electron transfer for electrochemically activated multiwalled carbon nanotubes and that the driving mechanism of the increased heterogeneous electron-transfer rate lies in an increase of the density of edge-like sites at the walls of MWCNTs.

Raman Spectroscopy

Raman spectroscopy plays an important role in the structural characterization of sp^2-hydrized carbon materials, providing information about defects and crystalline structure.[35–41] The most prominent features of Raman spectra of carbon nanotube materials are the so-called G band appearing at around 1580 cm^{-1} and the D band at around 1350 cm^{-1}. The G band is a doubly degenerated phonon Raman active mode for sp^2-hydrized carbon networks, whereas the D band is localized where the lattice structure is not perfect, mostly at the edges and defects of the sp^2 zones. Amorphization of sp^2-hydridized carbon networks, which leads to sp^3 hybridization, results in significant changes in the Raman profiles.[35,37,38] The ratio of the intensity of the G band to that of the D band (the so called "G/D ratio") is usually used for characterizing the quantity of defects in graphitic and carbon nanotube materials.[35,39–41]

Figure 4 shows the evolution of the G/D ratio with applied electrochemical activation potential (Figure 4A) and

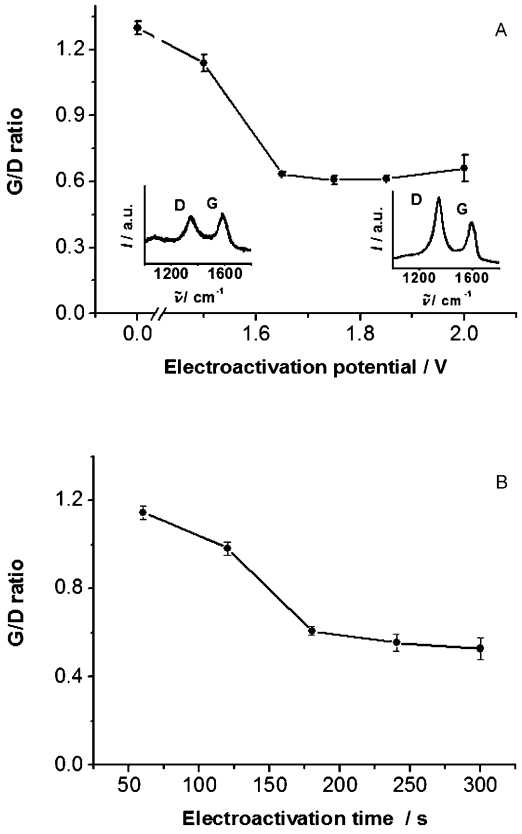

Figure 4. A) Effect of electrochemical activation potential on G/D ratio of carbon nanotubes after their electrochemical activation for 180 s. The inset shows the Raman spectra for as-received (left) and electrochemically activated carbon nanotubes for 180 s at 1.75 V (right). B) Effect of electrochemical activation time on G/D ratio of carbon nanotubes after their electrochemical activation at potential 1.75 V. Error bars correspond to standard deviation for $n=3$.

activation time (Figure 4B). Also shown are Raman spectra of as-received carbon nanotubes and electrochemically activated nanotubes at a potential of 1.75 V for 180 s (Figure 4A, insets). The G/D ratio decreases rapidly from 1.30 to 0.63 upon changes in the electrochemical activation potential from 0 to 1.65 V and then more slowly, reaching a minimum of 0.61 at an activation potential of 1.75 V and then increasing slightly to 0.66 at an activation potential of 2.00 V. A similar reversal of the G/D ratio was observed previously for radiation damage of HOPG, which first resulted to defects in the HOPG lattice, then to amorphization of the HOPG lattice.[38,39] Similar defects were observed for the MWCNTs as well.[41] Amorphization of the defect sites was observed in our samples by HR-TEM. Therefore, electrochemical activation leads not only to the creation of defects in the sp^2-hybridized structure of carbon nanotubes but also results in the amorphization of the defect sites of CNTs.

When the activation potential is fixed at 1.75 V and electrochemical activation time is changed, the G/D ratio decreases monotonically from 1.15 to 0.53 as the activation time is increased from 60 to 300 s (Figure 4B).

High-Resolution Transmission Electron Spectroscopy

Since cyclic voltammetry and electrochemical impedance spectroscopy provide evidence of increasing "edge-plane-like" defects in the structure of MWCNTs, we used HR-TEM to investigate the nature of these defects. Figure 5 shows representative TEM images of MWCNTs before (A) and after (B) electrochemical activation at 1.75 V for 180 s. The as-received MWCNT sample contains a straight, open-ended MWCNT with no visible structural defects. In contrast, the TEM image of the electrochemically activated nanotubes shows a striking difference. The structure of the MWCNT is damaged and wall defects can be observed. This damage is shown in greater detail in the HR-TEM images of the MWCNT after electroactivation at 1.65 V (Figure 6), 1.75 V (Figure 7A), and 1.85 V (Figure 7B). Electrochemical activation results in lattice damage of the MWCNT walls (Figure 6B), and the edge planes of the damaged graphene sheets are accessible through the outside environment (i.e.,

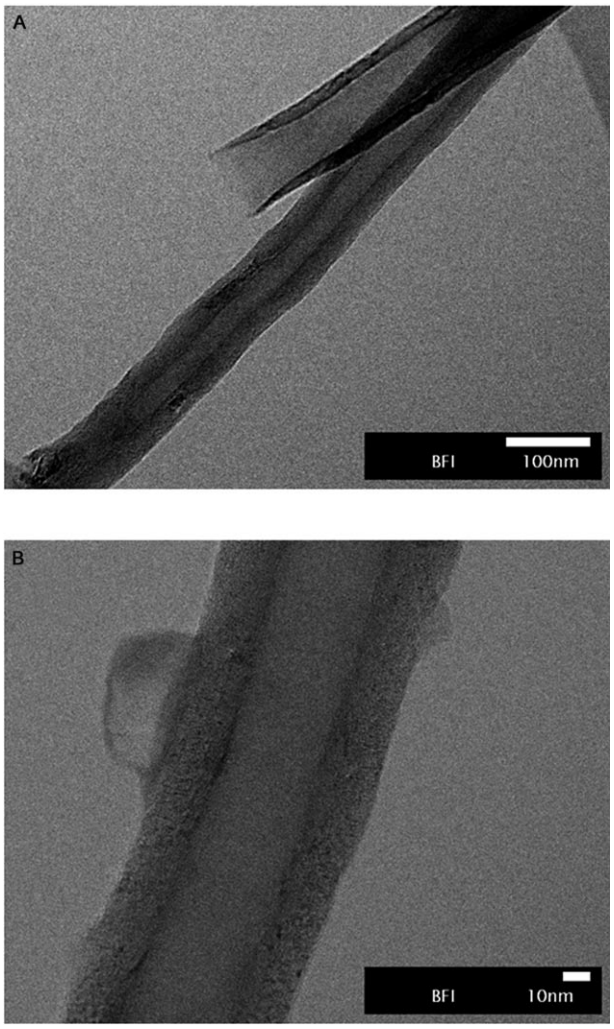

Figure 5. TEM images of A) as-received carbon nanotubes and B) carbon nanotubes electrochemically activated for 180 s at 1.75 V.

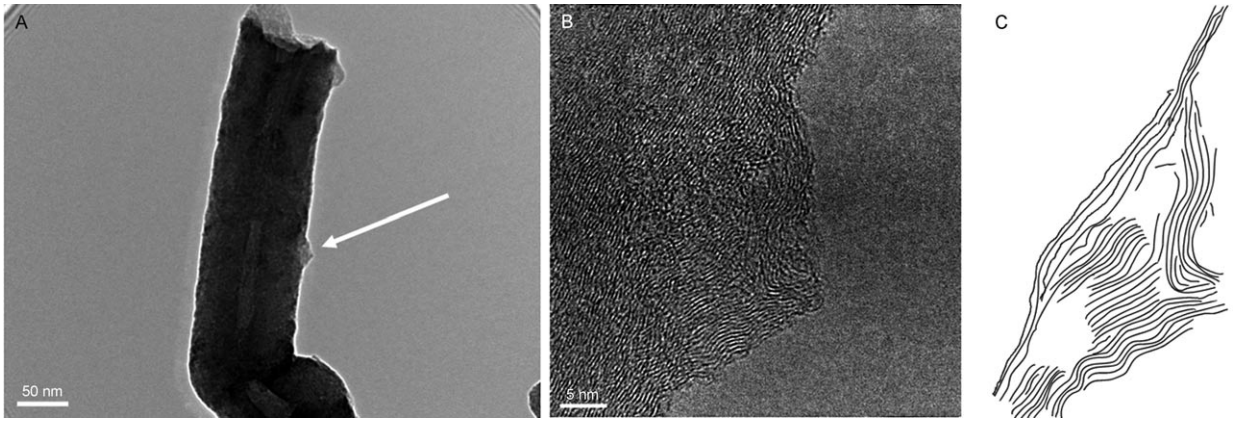

Figure 6. HR-TEM images of sidewall defects on carbon nanotubes electrochemically activated for 180 s at 1.65 V (vs. Ag/AgCl). The defect marked in (A) is shown in greater detail in (B). The lattice deformation of the MWCNT is clearly visible. For further clarity and emphasis on the deformation of the lattice, the important part of (B) is redrawn and is shown in (C). The white "vacancies" shown in (C) represent amorphous carbon.

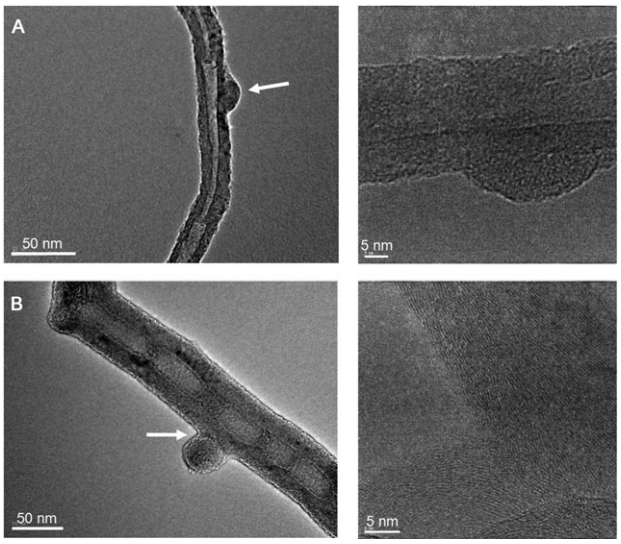

Figure 7. TEM (left) and HR-TEM (right) images of electrochemically activated MWCNTs at A) 1.75 V and B) 1.85 V for 180 s.

by solution). For greater clarity of the HR-TEM image, we redrew the main lattice lines (Figure 6C). Note that the white areas in Figure 6C represent parts of the MWCNT where the lattice is not observable, containing amorphous carbon, which was created during electroactivation. This observation of amorphous carbon is consistent with the Raman spectroscopic data. Another interesting point is that, with the application of increased electroactivation voltage, the size of these defects increases in a radial direction (compare the size of the defect sites in Figures 6 (activation potential 1.65 V), 7A (activation potential 1.75 V), and 7B (activation potential, 1.85 V)).

From the HR-TEM, Raman spectroscopy, electrochemical impedance spectroscopy, and cyclic voltammetry data, there are clear structure–reactivity correlations. With increased electrochemical activation potential, the magnitude of the defects on the MWCNT walls increases, leading to higher density of "edge-like" planes and therefore to a higher observed heterogeneous electron-transfer rate.

Density of Defects

How many defects are responsible for the observed increase in the value of k^0_{obs}? This is an important and interesting question. To determine a more quantitative relationship between the heterogeneous electron-transfer rate and the density of defects in the carbon nanotube structure, we used the approach for calculating the density of defects on the basis of electrochemistry and capacitance measurements developed by Yeager and Randin[42–44] and later by McCreery and Rice[18] for HOPG electrodes. Since we concluded in the previous sections of this article from electrochemistry, spectroscopy, and electron microscopy that electrochemical activation involves formation of "edge-like" defects on the walls of carbon nanotubes, we can propose the following way of determining the density of such defects.

If we hypothesize that k^0_{obs} in the first approximation is exclusively a function of the edge-plane density[18] of carbon nanotubes, and that k^0_{obs} is the weighted sum of the edge plane and basal plane k^0 values, we can write Equation (1), in which k^0_e is the heterogeneous electron-transfer rate constant of the pure edge plane, k^0_b is the heterogeneous electron-transfer rate constant of the pure basal plane, and f_e is the ratio of the edge planes to the basal planes. The literature values of k^0_e and k^0_b for HOPG are 0.10 $cm\,s^{-1}$ and 1×10^{-7} $cm\,s^{-1}$, respectively.[18] Even though the value of k^0_b might be less than 1×10^{-7} $cm\,s^{-1}$, probably in the region of 10^{-9} $cm\,s^{-1}$ or lower,[18,45] since k^0_e is much larger then k^0_b, the contribution of k^0_b to k^0_{obs} in Equation (1) is negligible for electrochemically activated MWCNTs and the accuracy of k^0_b is unimportant for determining f_e from Equation (1).[18] Since the electrochemistry of multiwalled carbon nanotube electrodes closely resembles the electrochemistry of HOPG electrodes,[12,46] one can use values of k^0_e and k^0_b of 0.10 and 1×10^{-7} $cm\,s^{-1}$, respectively, to calculate f_e. The values of f_e determined by this method [using Eq. (1) and data for k^0_{obs} presented in Figure 1] are shown in Figure 8 for different electrochemical activation potentials (A) and different electroactivation times (B). The increase of the frequency of defects from 0.083% for as-received MWCNTs to 2.5% for electrochemically activated MWCNTs (at 1.5 V for 180 s) is responsible for the steep increase in the value of k^0_{obs} by almost two orders of magnitude (from 8.34×10^{-5} to 2.54×10^{-3} $cm\,s^{-1}$; see section on "Cyclic Voltammetry"). A further increase of electrochemical activation potential from 1.5 to

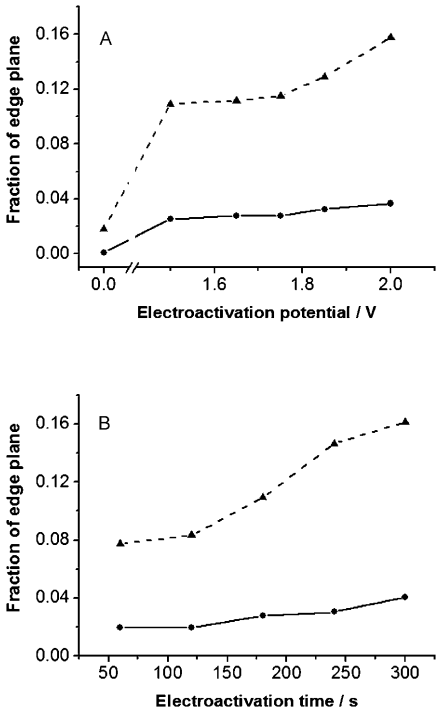

Figure 8. Plots of fraction of edge-plane defects on A) electrochemical activation potential and B) electroactivation time calculated from k^0_{obs} using Equation (1) and data from Figure 1 (circles) and from capacitance measurements using Equation (2) and data from Figure 2 (triangles).

2 V results in a relatively small increase in the frequency of defects (from 2.5 to 3.7%). Similarly, the density of defects increases for different electroactivation times from 2.0 to 4.0% for electroactivation times increasing from 60 to 360 s (electroactivation potential of 1.75 V). These results are consistent with our TEM images, in which it is not possible to see a significant difference in the density of defects on the surfaces of MWCNTs activated at different potentials, and the density of such TEM-observable defects is relatively low.

$$k^0_{obs} = k^0_e f_e + k^0_b(1 - f_e) \quad (1)$$

The density of defects can also be calculated from capacitance measurements, which can be used for estimating the presence of oxygen-containing groups and their influence on the observed capacitance. If we make the same hypothesis for observed area-specific capacitance ($C^0_{A,obs}$) as we did for k^0_{obs}, that is, that the observed capacitance is an exclusive function of edge plane density,[18] we can derive Equation (2), in which C^0_e is the capacitance per area of pure edge plane, C^0_b is the capacitance per area of pure basal plane, and f_e is the ratio of the edge planes to the basal planes.

$$C^0_{A,obs} = C^0_e f_e + C^0_b(1 - f_e) \quad (2)$$

It has been shown for laser-treated HOPG that the determination of the ratio of the coverage of the edge plane to the basal plane (f_e) from k^0_{obs} and C^0_{obs} data is quantitatively consistent, provided that no oxygen-containing groups are involved in contributing to the observed capacitance.[18] However, if oxygen-containing groups are present, they can contribute in various ways (see section on "Electrochemical Impedance Spectroscopy") to the observed capacitance. One can use this difference to determine the role of oxygen-containing groups in the capacitance of MWCNTs: if there is no contribution of oxygen-containing groups to f_e, the values of f_e calculated from k^0_{obs} and C^0_{obs} data by Equations (1) and (2) will be quantitatively consistent. However, if oxygen-containing groups contribute to the observed capacitance, the values of f_e calculated from C^0_{obs} and Equation (2) will be higher than those calculated from k^0_{obs} and Equation (1).

We used the values in the literature for C^0_e and C^0_b for HOPG (1.9 $\mu F\,cm^{-2}$ and 70 $\mu F\,cm^{-2}$, respectively)[18] and we converted the observed weight-specific capacitance ($C^0_{w,obs}$) of MWCNTs (presented in Figure 2) into area-specific capacitance ($C^0_{A,obs}$) by using data from surface-specific measurements of MWCNTs. From these data, we calculated f_e from Equation (2) as a function of electrochemical activation potential (Figure 8A, circles) and electrochemical activation time (Figure 8B, circles). As can be seen in Figure 8, f_e values based on capacitance measurements increase from 1.8% in as-received carbon nanotubes to 15.8% in carbon nanotubes that were electrochemically activated at 2.00 V for 180 s. Similarly, the frequency of defects calculated from capacitance measurements increases for different electroactivation times (at a potential of 1.75 V) from 7.7 to 16.1% with increasing electroactivation time from 60 to 360 s. It is clear that the values of the ratio of edge plane calculated from the k^0_{obs} data and capacitance data have the same trend (i.e., monotonous increase), but quantitatively the values differ significantly. Thus, there is considerable contribution from oxygen-containing groups to the observed capacitance of MWCNTs and the capacitance of MWCNTs is not solely a function of edge-plane defects. On the contrary, in our study, the oxygen-containing groups play a major role in determining the capacitance of MWCNTs (see section on "Electrochemical Impedance Spectroscopy").[18]

Conclusions

We have demonstrated that electrochemical activation of MWCNTs results in an increase in the observed heterogeneous electron-transfer rate constants for ferri/ferrocyanide couples, and the electrochemical activity of MWCNTs may be altered to any value between that of the as-received and exhaustively activated sample. By using HR-TEM, Raman spectroscopy, and electrochemical impedance spectroscopy, we proved that this increase is due to the introduction of dramatic edge-like defects to carbon nanotube walls during electrochemical activation. We calculated that small increases in the density of defects are responsible for a huge increase in the value of k^0_{obs}. We showed that the capacitance of MWCNTs is not solely the function of edge-plane defects, but that oxygen-containing groups play a major role. Detailed XPS analysis proved that during electrochemical activation, there is a significant increase in the presence of oxygen-containing groups and, most notably, carboxy groups. Our findings should find a broad range of applications in the areas of sensing, biosensing, and energy storage.

Experimental Section

Apparatus

A JEM 2100F field emission transmission electron microscope (JEOL, Japan) working at 200 kV was employed to obtain TEM images in a scanning TEM mode (spot size, 0.4 nm; 200 kV). HR-TEM images were obtained by using the same JEM 2100F microscope in conventional TEM mode. TEM/energy-dispersive X-ray spectra (TEM/EDS) were collected by using the above-described JEM 2100F instrument equipped with an ultrathin window. Raman spectra were collected by excitation at 514.5 nm with an Ar ion laser beam employing backscattering geometry (BeamLok 2060-RS/T64000, Spectro-Physics, Mountain View, CA/Jobin Yvon, Horiba, France). Surface specific areas were measured by Autosorb 1 equipment (Quantachrome Instruments, Boynton Beach, FL, USA) using the multipoint Brunauer–Emmett–Teller (BET) method[47] (60 points); nitrogen was used as the adsorbate. Prior to the adsorption experiments, the samples were dehydrated at 250°C under vacuum for 16 h. Thermogravimetric analysis (TGA) was performed on Exstar TG/DTA 6200 equipment (SII NanoTechnology, Japan) by placing the sample in the furnace with an air atmosphere, heating to 120°C at a heating rate of 10°C min^{-1}, holding at 120°C for 30 min to remove any moisture, and then heating again to 1000°C at a heating rate of 10°C min^{-1}.

All voltammetric experiments were performed on an electrochemical analyzer Autolab 302 (Ecochemie, Utrecht, The Netherlands) connected to a personal computer and controlled by General Purpose Electrochemical Systems v. 4.9 software (Ecochemie). The electrochemical experiments were performed in a 5 mL voltammetric cell at room temperature (25 °C) in a three-electrode configuration. A platinum electrode served as the auxiliary electrode and a Ag/AgCl electrode as the reference electrode. Electrochemical impedance spectroscopy was performed by using an Autolab 302 electrochemical analyzer equipped with an FRA2 module and operated by FRA 4.9 software (Ecochemie). X-ray photoelectron spectroscopy (XPS) was performed on a PHI Quantera SXM (ULVAC-PHI) spectrometer with monochromatic $Al_{K\alpha}$ radiation. The analysis area was 50 μm in diameter and the beam energy was 15 kV, 12.5 W; the photoelectron take-off angle was 45°. For the HR-XPS scans, the pass energy was 13 eV and steps of 0.1 eV. XPS is a highly surface-sensitive method and the sensitivity strongly decreases with depth (the maximum depth for carbon analysis is about 10 nm).

Materials

Potassium chloride, potassium phosphate (dibasic), potassium ferrocyanide, potassium ferricyanide, and phosphoric acid were purchased from Sigma–Aldrich (Japan). Multiwalled carbon nanotubes were purchased from Bucky, TX, USA (BU-200, purity measured by TGA was 99.2 % wt.; surface-specific area 37.61 $m^2 g^{-1}$; diameter 8–15 nm, length 5–10 μm, according to the producer) and used as received. TEM/EDS analysis of metal impurities was performed by using a JEM 2100F transmission electron microscope with an EDS module and showed that BU-200 contains iron impurities within the carbon nanotube (see Figure S-3 in the Supporting Information).

Procedures

Carbon nanotube materials were used as received without further purification. For the electrochemistry measurements, the carbon nanotubes were cast onto a glassy carbon (GC) electrode surface (3 mm in diameter, surface area 0.071 cm^2, received from Autolab), which was previously polished with 0.05 μm alumina on a polishing cloth. The nanotubes were first dispersed in DMF at a concentration of 1 $mg mL^{-1}$, and the suspension was then placed for 5 min into an ultrasonic bath and then 5 μL of the suspension was pipetted onto the GC electrode surface. (The surface area of the deposited MWCNT was 1.88 cm^2, according to our measurements by the BET method). The suspension was allowed to evaporate at room temperature to create a MWCNT film over the entire GC electrode surface. The contribution of the underlying GC electrode to the electrochemical response is considered negligible[19,20] because the surface area of the deposited MWCNT is 1.88 cm^2, whereas the surface area of the GC electrode is 0.071 cm^2. Thus the surface area of the deposited MWCNT layer is at least 26 times greater than that of the GC electrode and most electron transfer occurs on the MWCNT layer. If not stated otherwise, the cyclic voltammetric experiments were performed at a scan rate of 100 $mV s^{-1}$ over a relevant potential range using 0.1 M KCl as a supporting electrolyte. Capacitance was determined by electrochemical impedance spectroscopy measurements in the frequency range of 0.01 Hz and 1 MHz with a perturbation signal of 5 mV. The capacitance values were extracted by fitting Nyquist plots using Randles equivalent circuit shown as the inset in Figure 2. If not stated otherwise, 10 mM $[Fe(CN)_6]^{3-/4-}$ was used as an electrochemical probe. For TEM measurements, MWCNTs were mechanically removed from the GC electrode surface by using a plastic pipette tip and transferred to a drop of water. This droplet was transferred onto a copper TEM grid and allowed to dry in air. For XPS and Raman measurements, MWCNTs were transferred from the electrode surface to the corresponding substrate by the above-described procedure.

The k^0_{obs} values were determined by the method developed by Nicholson[23] that relates ΔE_p to dimensionless parameter ψ and consequently to k^0_{obs} through Equation (3), in which k^0_{obs} is observed heterogeneous rate constant, D_A is the diffusion coefficient, ν is the scan rate, F is the Faraday constant, R is the gas constant, and T is the absolute temperature.

$$k^0_{obs} = \psi\sqrt{\pi D_A \nu \frac{nF}{RT}} \quad (3)$$

The value of parameter ψ and a detailed discussion on the use of this equation can be found in reference [23]. A diffusion coefficient for $[Fe(CN)_6]^{3-}$ in 0.1 M KCl of 7.2×10^{-6} $cm^2 s^{-1}$ was used for evaluation of all electrochemical data. Since all k^0_{obs} data are obtained by either interpolation (for ΔE_p between 60 and 242 mV) or extrapolation (for $\Delta E_p >$ 242 mV) of Nicholson's working curve,[23] an additional interpolation/extrapolation error of approximately 0–2 % is introduced in addition to an experimental error of ΔE_p.

[1] A. Oberlin, M. Endo, T. Koyama, *J. Cryst. Growth* **1976**, *32*, 335–349.
[2] S. Iijima, *Nature* **1991**, *354*, 56–58.
[3] D. S. Bethune, C. H. Kiang, M. S. De Vries, G. Gorman, R. Savoy, J. Vazquez, R. Beyers, *Nature* **1993**, *363*, 605–607.
[4] S. Iijima, T. Ichihashi, *Nature* **1993**, *363*, 603–605.
[5] M. J. Esplandiu, M. Pacios, E. Bellido, M. del Valle, *Z. Phys. Chem.* **2007**, *221*, 1161–1173.
[6] J. Wang, *Electroanalysis* **2005**, *17*, 7–15.
[7] J. J. Gooding, *Electrochim. Acta* **2005**, *50*, 3049–3060.
[8] M. Pumera, S. Sánchez, I. Ichinose, J. Tang, *Sens. Actuators B* **2007**, *123*, 1195–1205.
[9] A. Merkoçi, M. Pumera, X. Llopis, B. Perez, M. del Valle, S. Alegret, *TrAC Trends Anal. Chem.* **2005**, *25*, 826–838.
[10] C. E. Banks, R. G. Compton, *Analyst* **2006**, *131*, 15–21.
[11] J. M. Nugent, K. S. V. Santhanam, A. Rubio, P. M. Ajayan, *Nano Lett.* **2001**, *1*, 87–91.
[12] C. E. Banks, T. J. Davies, G. G. Wildgoose, R. G. Compton, *Chem. Commun.* **2005**, 829–841.
[13] A. Chou, T. Böcking, N. K. Singh, J. J. Gooding, *Chem. Commun.* **2005**, 842–844.
[14] M. Pumera, *Langmuir* **2007**, *23*, 6453–6458.
[15] R. J. Bowling, R. T. Packard, R. L. McCreery, *J. Am. Chem. Soc.* **1989**, *111*, 1217–1223.
[16] C. A. Goss, J. C. Brumfield, E. A. Irene, R. W. Murray, *Anal. Chem.* **1993**, *65*, 1378–1389.
[17] A. A. Gewirth, A. J. Bard, *J. Phys. Chem.* **1988**, *92*, 5563–5566.
[18] R. J. Rice, R. L. McCreery, *Anal. Chem.* **1989**, *61*, 1637–1641.
[19] J. Wang, M. Li, Z. Shi, N. Li, Z. Gu, *Anal. Chem.* **2002**, *74*, 1993–1997.
[20] M. Musameh, N. S. Lawrence, J. Wang, *Electrochem. Commun.* **2005**, *7*, 14–18.
[21] T. Ito, L. Sun, R. M. Crooks, *Electrochem. Solid-State Lett.* **2003**, *6*, C4–C7.
[22] C.-M. Liu, H.-B. Cao, Y. P. Li, H. B. Xu, Y. Zhang, *Carbon* **2006**, *44*, 2919–2924.
[23] R. S. Nicholson, *Anal. Chem.* **1965**, *37*, 1351–1355.
[24] T. Kim, S. Lim, K. Kwon, S.-H. Hong, W. Qiao, C. K. Rhee, S.-H. Yoon, I. Mochida, *Langmuir* **2006**, *22*, 9086–9088.
[25] Z. Wang, N. Koratkar, L. Ci, P. M. Ajayan, *Appl. Phys. Lett.* **2007**, *90*, 143117–143119.
[26] N. S. Lawrence, R. P. Deo, J. Wang, *Electroanalysis* **2005**, *16*, 65–72.
[27] J. Li, A. Cassell, L. Delzeit, J. Han, M. Meyyappan, *J. Phys. Chem. B* **2002**, *106*, 9299–9305.
[28] M. Pumera, *Nanoscale Res. Lett.* **2007**, *2*, 87–93.
[29] M. Liu, Y. Yamg, T. Zhu, Z. Liu, *Carbon* **2005**, *43*, 1470–1478.
[30] T. I. T. Okpalugo, P. Papakonstantinou, H. Murphy, J. McLaughlin, N. M. D. Brown, *Carbon* **2005**, *43*, 153–161.
[31] M. Pumera, B. Šmíd, *J. Nanosci. Nanotechnol.* **2007**, *7*, 3590–3595.
[32] A. T. Masheter, L. Xiao, G. C. Wildgoose, A. Crossley, J. H. Jones, R. G. Compton, *J. Mater. Chem.* **2007**, *17*, 3515–3524.
[33] X. Ji, C. E. Banks, A. Crossley, R. G. Compton, *ChemPhysChem* **2006**, *7*, 1337–1344.
[34] C. E. Banks, X. Ji, A. Crossley, R. G. Compton, *Electroanalysis* **2006**, *17*, 2137–2140.

[35] A. Pimenta, G. Dresselhaus, M. S. Dresselhaus, L. G. Cançado, A. Jorio, R. Saito, *Fortschr. Chem. Phys. Phys. Chem.* **2007**, *9*, 1276–1291.
[36] F. Tuinstra, J. L. Koenig, *J. Chem. Phys.* **1970**, *53*, 1126–1131.
[37] T. Tanabe, *Phys. Scr.* **1996**, *64*, 7–16.
[38] A. C. Ferrari, J. Robertson, *Phys. Rev. B* **2000**, *61*, 14095–14107.
[39] K. Kordás, T. Mustonen, G. Toth, H. Jantunen, M. Lajunen, C. Soldano, S. Talapatra, S. Kar, R. Vajtai, P. M. Ajayan, *Small* **2006**, *2*, 1021–1025.
[40] M. Pumera, B. Šmíd, X.-S. Peng, J. Tang, I. Ichinose, *Chem. Eur. J.* **2007**, *13*, 7644–7649.
[41] S. Gupta, R. J. Patel, *J. Raman Spectrosc.* **2007**, *38*, 188–199.
[42] J. P. Randin, E. Yeager, *J. Electrochem. Soc.* **1971**, *118*, 711–714.
[43] J. P. Randin, E. Yeager, *J. Electroanal. Chem.* **1972**, *36*, 257–276.
[44] J. P. Randin, E. Yeager, *J. Electroanal. Chem.* **1975**, *58*, 313–322.
[45] T. J. Davies, M. E. Hyde, R. G. Compton, *Angew. Chem.* **2005**, *117*, 5251–5256; *Angew. Chem. Int. Ed.* **2005**, *44*, 5121–5126.
[46] C. E. Banks, R. R. Moore, T. J. Davies, R. G. Compton, *Chem. Commun.* **2004**, 1804.
[47] S. Brunauer, P. H. Emmett, E. Teller, *J. Am. Chem. Soc.* **1938**, *60*, 309–319.

Received: May 26, 2008
Revised: July 17, 2008
Published online: September 22, 2008

